

Journal of Materials Chemistry C

Accepted Manuscript



This is an *Accepted Manuscript*, which has been through the Royal Society of Chemistry peer review process and has been accepted for publication.

Accepted Manuscripts are published online shortly after acceptance, before technical editing, formatting and proof reading. Using this free service, authors can make their results available to the community, in citable form, before we publish the edited article. We will replace this *Accepted Manuscript* with the edited and formatted *Advance Article* as soon as it is available.

You can find more information about *Accepted Manuscripts* in the [Information for Authors](#).

Please note that technical editing may introduce minor changes to the text and/or graphics, which may alter content. The journal's standard [Terms & Conditions](#) and the [Ethical guidelines](#) still apply. In no event shall the Royal Society of Chemistry be held responsible for any errors or omissions in this *Accepted Manuscript* or any consequences arising from the use of any information it contains.

Dibenzo[*a,e*]pentalene-Embedded Dicyanomethylene-Substituted Thienoquinoidals for n-Channel Organic Semiconductors: Synthesis, Properties, and Device Characteristics

Cite this: DOI: 10.1039/x0xx00000x

Received 00th January 2012,
Accepted 00th January 2012

DOI: 10.1039/x0xx00000x

www.rsc.org/

Masahiro Nakano,^a Itaru Osaka,^a and Kazuo Takimiya^{*a,b}

Dibenzo[*a,e*]pentalene-embedded thienoquinoidals with dicyanomethylene termini were synthesized as a new π -extended thienoquinoidals for n-type organic semiconductors. Single crystal X-ray analysis demonstrated that the target molecule has all *trans*-polyene structure with reasonable bond-length alternation in the thienoquinoidal strand, indicative of effective extension of π -conjugation system. Thanks to their π -extended structures, not just the low-lying LUMO energy levels ($-4.2\sim-4.3$ eV) but also relatively high HOMO energy levels (~ 5.6 eV) were characterized by means of cyclic voltammetry. Interestingly, depending on the position of the solubilizing long alkyl groups, they formed H- or J- aggregate-like structures in the thin-film state testified by the thin film absorption spectra. These distinct intermolecular interactions in the thin film state could cause different behaviours in thin-film field-effect transistors; for the former ambipolar characteristics were observed, whereas only n-type response was detected for the latter.

Introduction

Considerable interests have been focused on functional π -materials for their potential applications in electronic devices, such as organic field-effect transistors (OFETs) and organic photovoltaics (OPVs).¹ OFETs have been attracting substantial attention because of their potential use in a variety of practical devices, e.g., back planes for active matrix displays and radio frequency identifier (RFID) tags.² The majority of high-performance OFETs has been of p-type, where the hole is the active carrier in the channel. Although recent intensive research efforts have realized several n-type OFETs with mobility approaching to those in the p-type OFETs, the development of n-type organic semiconductors is still lagged behind in terms of performances and materials diversity.³ Thus, to explore the materials being potential as n-type organic semiconductors is an important issue in the materials science.

The principal design strategy for developing n-type organic semiconductors is to realize a low-lying energy level of the lowest unoccupied molecular orbital (LUMO), and to this end, several molecular systems with electron deficient nature, such as rylene diimides,⁴ fullerene derivatives,⁵ fluoro-substituted aromatics,⁶ have been examined. Dicyanomethylene-substituted quinoidal compounds, first developed as electron acceptors for conductive charge-transfer salts in 1960s,^{7,8} have low-lying LUMOs owing to the quinoidal structure and cyano groups with strong electron withdrawing nature. They have been therefore thought to be a potential material class for n-type organic semiconductors applicable in n-type OFETs,⁹ and in fact, several dicyanomethylene-substituted quinoidal compounds, in particular, the thienoquinoidal-based compounds (**1–6**)^{10–12} have demonstrated promising characteristics with field-effect electron mobility as high as $0.9\text{ cm}^2\text{ V}^{-1}\text{ s}^{-1}$.^{10b} In such dicyanomethylene-terminated thienoquinoidal compounds for OFET applications, extension of the π -conjugated system is the most

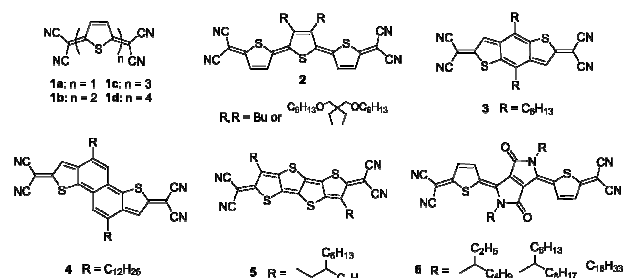


Figure 1. Molecular structure of dicyanomethylene-terminated thienoquinoidal molecules.

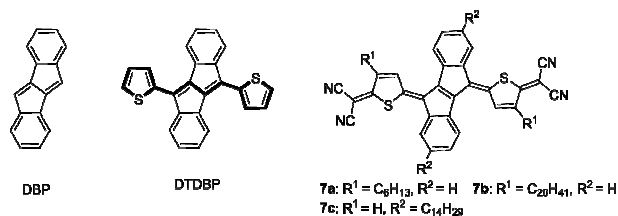


Figure 2. Chemical structures of dibenzo[*a,e*]pentalene (DBP), 5,10-di(2-thienyl)dibenzo[*a,e*]pentalene (DTDBP), and 7.

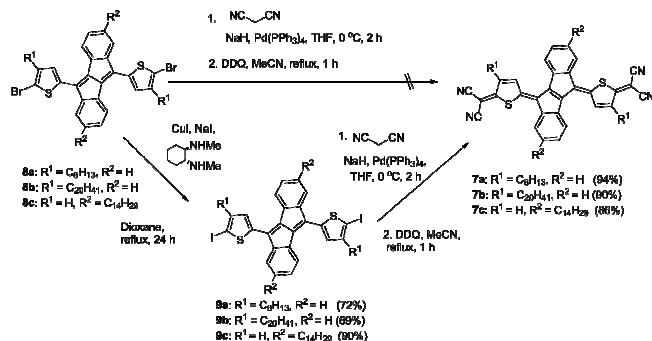
important approaches to attain high mobility.^{11b,12a,b}

There can be several ways to effectively extend the thiophene-based π -conjugated system, e.g., constructing oligomers (e.g., **1b–1d** and **2**)¹⁰ or fused-systems (thienoacene structures, e.g., **3–5**),¹¹ which have been already examined in the development of thienoquinoidal systems. Insertion of different π -systems is another way to extend the conjugation system.¹² In the present work, we designed dibenzo[*a,e*]pentalene (DBP)¹³-included thienoquinoidals (Figure 2) as new potential n-type organic semiconductors for following reasons. As we already demonstrated in a recent paper, a 5,10-dithienyl-DBP (DTDBP) moiety can act as a “benzo-annulated” 1,4-dithienyl-1,3-butadiene moiety in the conjugated molecules, where the two thiophene rings are effectively connected in a single conjugation path,^{13b} and thus the resulting target molecules (**7**) should have a largely extended quinoidal system (Figure 2). Also the annulated benzene ring can define the polyene strand in all-*trans* structure, which can eliminate possible isomerization in the case of simple polyene connected system. In fact, similar diketopyrrolopyrrole-embedded thienoquinoidal compounds (**6**)^{12a,b} have recently been reported to show high electron mobilities. We here describe the synthesis, physicochemical properties, and crystal structures of DBP-embedded thienoquinoidals as new organic semiconductors with a low-lying LUMO energy level.

Result and discussion

Synthesis and structural characterization

The synthesis of **7a–c** is shown in Scheme 1. A general synthetic strategy using the palladium-catalyzed Takahashi reaction¹⁴ for dicyanomethylene-terminated quinoidal compounds was first applied to the corresponding dibrominated precursor, 5,10-bis[2-(5-bromo-4-alkyl)thiophen-2-yl]dibenzo[*a,e*]pentalene (**8a** and **8b**)^{13b} and 5,10-bis[2-(5-bromo)thiophen-2-yl]-2,7-ditradecyldibenzo[*a,e*]pentalene (**8c**). The formers were prepared according to the reported procedure, whereas the latter was synthesized from 2,7-dibromo-5,10-dihydrodibenzo[*a,e*]pentalene-5,10-dione (Scheme S1). With the bromides (**8a–c**) as substrates, the reaction, however, did not proceed at all, and **8a–c** were recovered, which was surprising, since in general the syntheses of dicyanomethylene-terminated thienoquinoidal compounds have been successfully done by this method. The reasons for poor reactivity of the present substrates are not clear, but we anticipate that the DBP part in **8** can act as a kind of ligand owing to the 10π anti-aromatic nature of the central pentalene part, resulting in reducing reactivity in the reaction.



Scheme 1. Synthesis of **7**.

Alternatively, the corresponding diiodides (**9a–c**), which were readily converted from **8a–c** through a copper-catalyzed halogen exchange reaction,¹⁵ were smoothly reacted to afford the corresponding bis(dicyanomethyl) intermediates, which were further oxidized to produce **7a–c** in high yields.

Although **7a** with hexyl groups on the thiophene rings has poor solubility (~ 0.08 g L⁻¹ in chloroform), **7b** and **7c** were soluble in common organic solvents (e.g., > 3.0 g L⁻¹ in chloroform at rt) thanks to their long alkyl groups. The structures of **7** were fully characterized by spectroscopic analysis (see experimental section for detail). To our surprise, only one singlet (**7a**: δ 7.98, **7b**: δ 7.99) or a pair of doublet (**7c**: δ 8.24 and 7.47 with $J = 5.3$ Hz) assignable to the β -hydrogen atoms in the terminal thiophene rings were observed in the ¹H NMR spectra. In fact, there can be three possible isomers of **7** depending on the connectivity between the DBP moiety and two thiophene moieties, i.e., *EE*, *EZ*, and *ZZ* isomers (Figure 3), which should give multiple peaks in the aromatic region of the ¹H NMR spectra. The simple ¹H NMR spectra are in fact strong evidence for the fact that there is no *E/Z* isomerism on **7** regardless of the position and length of alkyl substituents. To determine the molecular structure clearly, single-crystal X-ray analysis of **7a** was carried out. As depicted in Figure 4, **7a** is unambiguously defined as the *EE* isomer. It is likely that possible steric repulsion between the thiophene β -hydrogens and hydrogens at 1,6-positions of the DBP moiety in the *Z*-configuration can eliminate the formation of the *ZZ* and *EZ* isomers. In fact, similar selective formation of one of several isomers owing to steric effect have been reported for the related thienoquinoidal compounds.^{10i,12a,12b} Although the present *EE* isomer is the least sterically congested among the three isomers, the molecular structure is slightly twisted resulting in a saddle-like molecular structure (Figure 4a). Nevertheless, the C–C bond lengths in **7a** clearly show that the bond-length-alternation agrees well to the formal quinoidal structure (Figure 4b),^{12a,b} indicating that **7** is a fairly extended quinoidal system.

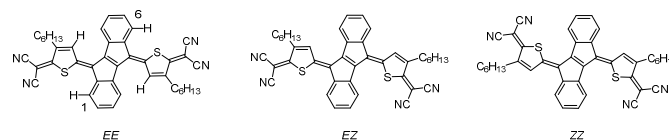


Figure 3. Possible isomers of **7a**.

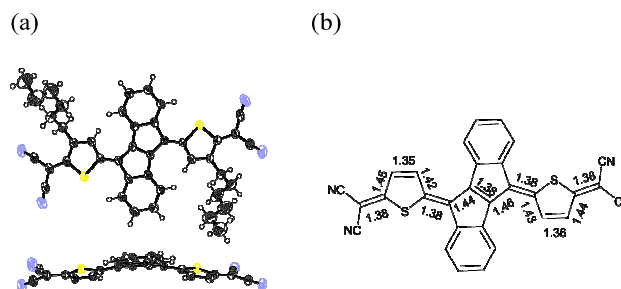


Figure 4. (a) X-ray crystallographic structures of **7a**; top view (top) and side view without hexyl groups for clarity (bottom) and (b) selected C–C bond lengths (Å).

Physicochemical properties

Although quantitative measurement of the absorption spectra of **7a** in solution was difficult owing to its poor solubility, the electronic structures of **7a** and **7b** possessing alkyl groups on the thiophene β -positions should be similar to each other as the shapes of their absorption bands are almost identical (Figure S1). On the other hand, the electronic structures of **7b** and **7c** were investigated by using cyclic voltammetry and absorption spectra in solution. The cyclic voltammograms of **7b** and **7c** showed similar redox behaviours to each other (Figure 5a, Table 1) with both oxidation and reduction waves in the typical electrochemical window (± 1.5 V vs. Ag/AgCl). From the redox onsets, it is expected that **7b** and **7c** have almost identical HOMO energy level (E_{HOMO} , -5.6 eV), whereas slightly different LUMO energy levels (E_{LUMOS}), -4.2 eV for **7b** and -4.3 eV for **7c**, respectively, were estimated. Comparison of these electrochemical E_{HOMOS} and E_{LUMOS} with those of bithienoquinoidal- (**1b**) and terthienoquinoidal counterpart (**1c**) as prototypical thienoquinoidal compounds indicates that the electronic structures of **7** is similar to those of **1c**, which can be rationalized by considering the extent of π -extension: both **7** and **1c** consists of the polyene strand with seven C=C double bonds between the dicyanomethylene termini.

The low-lying E_{LUMOS} of **7b** and **7c** meet the criteria for facile electron injection and transport under ambient conditions similar to other thienoquinoidal derivatives.¹⁰⁻¹² It is interesting to note that the slightly high-lying E_{LUMO} of **7b** than that of **7c** is reproduced by the theoretical DFT calculations of the corresponding model compounds (**7b'** and **7c'**), where the long alkyl groups are substituted by methyl groups (Figure 6).¹⁶ The schematic expression of the LUMO geometry indicates that the LUMO of **7** is mainly contributed by the thienoquinoidal strand, not by the benzene moiety, which implies that the alkyl groups of **7b'** at the thiophene β -positions may push the E_{LUMO} up by their electron donating nature. On the contrary, it is rational to consider that the alkyl groups on the benzene ring do not affect E_{LUMO} of **7c**, resulting in the slight difference in their E_{LUMOS} as well as electrochemical HOMO-LUMO gap (E_g).

The absorption spectra of **7b** and **7c** in solution (Figure 5b) exhibit an intensive absorption band at around 600 nm, and a long tail up to the near-infrared region. Likely reflecting smaller E_g of **7c** than **7b** electrochemically estimated, the absorption edge of **7c** is bathochromically shifted compared with that of **7b** (Figure 5b inset). These optical properties are nicely reproduced by the TD-DFT calculations on **7b'** and **7c'** (Figure S2, Table S1): the intense absorption bands at around

transition are almost the same (599 and 597 nm for **7b'** and **7c'**, respectively, with larger oscillator strengths, f_s , than 1.3), whereas the bands at the absorption edge mainly assignable to HOMO-LUMO transition were significantly different (890 nm with f of 0.09 and 985 nm with f of 0.06 for **7b'** and **7c'**, respectively).

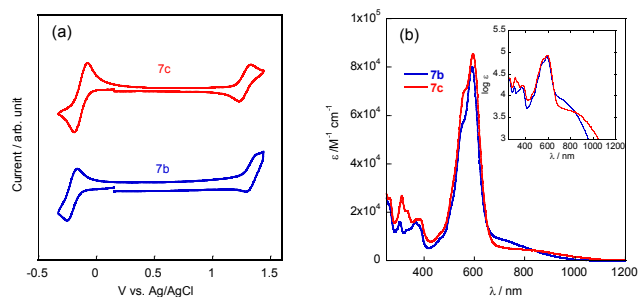


Figure 5. Cyclic voltammograms (a) and absorption spectra (b) of the CH_2Cl_2 solution of **7b** and **7c**.

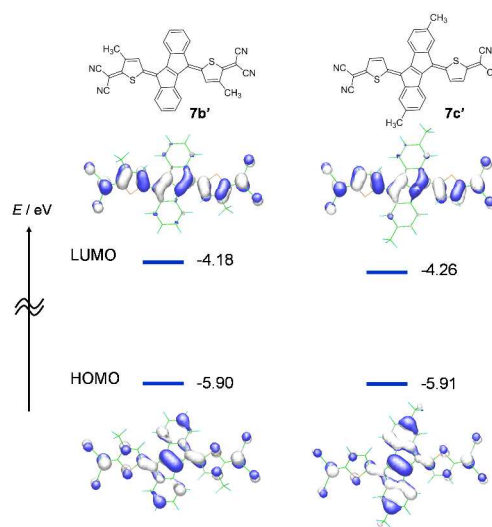


Figure 6. Calculated HOMO and LUMO of the model compounds of **7b** and **7c** (**7b'** and **7c'**, respectively) (B3LYP/6-31G* level).

Thin-film and OFETs

Thin-film deposition of **7b** and **7c** on quartz or octyltrichlorosilane (OTS)-treated Si/SiO₂ substrates was easily achieved by the spin-coating using THF solution (3 g L⁻¹), though it was difficult to deposit thin film of **7a** in good quality on the substrates owing to its poor solubility.¹⁷ The out-of-plane

Table 1. Electrochemical and optical properties of **7b** and **7c** in comparison with **1b** and **1c**.

compound	$E_{\text{ox}}^{1/2} / \text{V}^{\text{a}}$	$E_{\text{ox}}^{\text{onset}} / \text{V}^{\text{a}}$	$E_{\text{HOMO}} / \text{eV}^{\text{b}}$	$E_{\text{red}}^{1/2} / \text{V}^{\text{a}}$	$E_{\text{red}}^{\text{onset}} / \text{V}^{\text{a}}$	$E_{\text{LUMO}} / \text{eV}^{\text{b}}$	$\lambda_{\text{onset}} / \text{nm}$	$E_g^{\text{opt}} / \text{eV}$
7b	+1.32	1.24	-5.6	-0.21	-0.16	-4.2	950	1.3
7c	+1.28	1.22	-5.6	-0.13	-0.08	-4.3	1050	1.2
1b	–	–	–	-0.10, -0.32	-0.03	-4.4	647	2.0
1c	+1.35	+1.30	-5.7	-0.12	-0.04	-4.4	811	1.5

^a V vs. Ag/AgCl. All the potentials were calibrated with the Fc/Fc^+ ($E^{1/2} = +0.43$ V measured under identical conditions). ^b estimated with a following equation: E (eV) = $-4.4 - E_{\text{onset}}$. ^c calculated from λ_{onset} .

600 nm, mainly contributed from the HOMO-1 \rightarrow LUMO XRD patterns of the annealed films of **7b** and **7c** (100 °C, 30

min) showed a series of peaks, indicating formation of crystalline thin films (Figure 7a). The d -spacings extracted from the out-of-plane XRDs are 30.9 and 26.1 Å for **7b** and **7c**, respectively, implying that the d -spacing is strongly dependent on the length of alkyl groups, despite the different substitution position. Thus, edge-on molecular orientation with the alkyl groups standing on the substrate can be anticipated for the **7**-based thin films. Such edge-on orientation of semiconducting molecules in the thin film state is known to be suitable for facial charge transport in OFETs (vide infra).

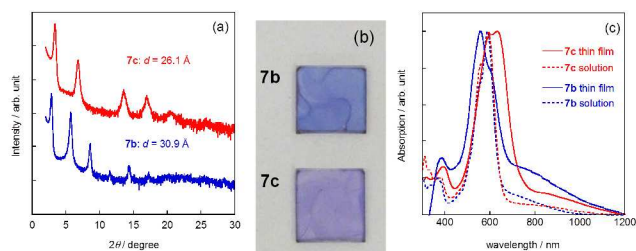


Figure 7. (a) Out-of-plane XRD patterns of the **7b**- and **7c**-thin films on Si/SiO₂ substrates. (b) Photographs of the **7b**- and **7c**-thin films on glass substrates. (c) normalized absorption spectra of **7b**- and **7c**-thin films deposited on quartz substrates (solid lines). Absorption spectra in solution are depicted in dotted lines for comparison.

Interestingly, the **7**-based thin films showed distinct colours (Figure 7b), which reflects the different absorption spectra of thin films (Figure 7c). Depending on the substitution positions of alkyl groups, different shifts in thin-film absorption spectra relative to the corresponding solution spectra were observed; for **7b** obvious blue shift of the major band (~ 600 nm) is characteristic, whereas the **7c** thin film shows red shift (Figure 7c). At the moment, these differences can not be clearly explained, but we anticipate that the alkylation position, not the length of alkyl groups, influences the mode of intermolecular interaction of the quinoidal core part of **7**; intermolecular van der Waals forces originating from the alkyl groups may determine mutual position of the quinoidal cores to interact,¹⁸ resulting in H- (**7b**) or J- (**7b**) aggregate-like interactions in the thin film state (Figure 8),¹⁹ which will be discussed later.

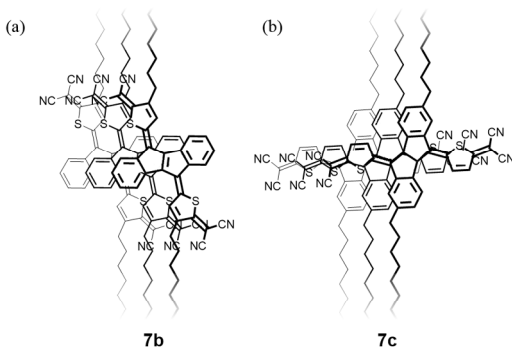


Figure 8. Schematic representation of intermolecular interactions for **7b** (a) and **7c** (b).

Bottom-gate, top-contact OFETs consisting of the spin-coated thin films as the active layer were evaluated under ambient conditions (Figure 9). Thanks to the low-lying E_{LUMOS} for both compounds, **7b**- and **7c**-based OFETs showed n-channel transistor characteristics. The extracted electron mobility from the saturation regime was of up to $4.8 \times 10^{-2} \text{ cm}^2 \text{ V}^{-1} \text{ s}^{-1}$ (**7b**) and $1.9 \times 10^{-2} \text{ cm}^2 \text{ V}^{-1} \text{ s}^{-1}$ (**7c**), respectively (Table 2), which are almost comparable or slightly lower than those related thienoquinoidal derivatives.¹⁰⁻¹² The moderate mobility of the present devices could partially be ascribed to the non-planar molecular core (Figure 4a) that can reduce the effective intermolecular interaction in the thin film state.

Although obvious ambipolar behaviour was not observed for the **7b**-based devices, weak hole transport was detected both in the transfer (negative V_g regime) and output characteristics ($V_g = 0$ V, $V_d = 60$ V) (Figure 9a). In fact, under p-channel operation conditions (largely negative V_d and V_g), clear but relatively poor p-channel behaviour was observed (Figure S3), which could be rationalized by considering its high-lying E_{HOMO} of -5.6 eV (Table 1). In sharp contrast, no sign of p-channel behaviour was detected for **7c**-based OFETs, even though its E_{HOMO} electrochemically estimated is virtually the same with that of **7b**. This marked difference can be related to their packing structures or the mode of intermolecular interactions in the thin film state; for **7b** the clear blue shift in the thin film absorption spectra relative to that in solution (Figure 7c) implies that the mode of intermolecular interaction can be H aggregate-like, in which molecular planes overlap without large offset in the molecular long axis direction, e.g., the direction along the quinoidal strand of **7** (Figure 8a).¹⁹ This mode can ensure effective

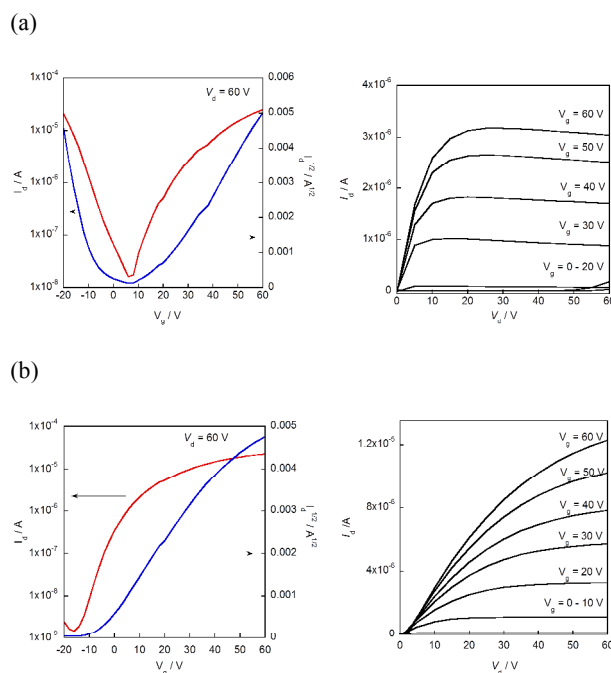


Figure 9. Transfer characteristics (left) and output curves (right) of **7b**- (a) and **7c**-based OFET devices (b).

intermolecular orbital overlaps of both LUMO and HOMO, to the latter of which the central DBP part largely contributes (Figure 6). On the other hand, J aggregate-like **7c** as evidenced by the red shift in thin film absorption spectra (Figure 7c) indicates that the packing structure of **7c** in the thin film state should have a relatively large offset along the quinoidal direction, reducing effective overlap at the central DBP part, likely resulting in reduction of effective intermolecular orbital overlap of HOMOs (Figure 8b). Being different from the HOMO, the quinoidal strand mainly contributes to the LUMO of **7** (Figure 6), which makes the intermolecular orbital overlap of LUMOs less sensitive to the molecular offset, though slight reduction of electron mobility in **7c**-based OFETs could be related. These results imply that the combination of molecular electronic structures having topologically separated HOMO and LUMO with dictation of intermolecular interaction by alkyl groups can give a chance to control carrier type in ambipolar organic semiconductors.

Table 2. OFET characteristics^a of **7b** and **7c**.

compound	Annealing conditions	$\mu_e / \text{cm}^2 \text{V}^{-1} \text{s}^{-1}$ ^b	$I_{\text{on}} / I_{\text{off}}$	V_{th} / V
7b	as spun	3.0×10^{-2}	1.8×10^3	+15
	100 °C, 30 min	4.8×10^{-2}	1.5×10^3	+14
7c	as spun	1.4×10^{-2}	1.6×10^4	-9
	100 °C, 30 min	1.9×10^{-2}	1.5×10^4	-10

^a Devices with bottom gate, top-contact configuration with $L = 50 \mu\text{m}$ and $W = 1500 \mu\text{m}$ fabricated on Si/SiO₂ substrates modified with octyltrichlorosilane (OTS) self-assembled monolayer (SAM) were used. ^b extracted from the saturation regime ($V_g = V_d = 60 \text{V}$) under ambient conditions.

Conclusion

Taking advantage of the all-*trans*-fixed 1,3-butadiene structure of 5,10-dithienyl-dibenzo[*a,e*]pentalene (DBP), we have successfully synthesized DBP-embedded thienoquinoidal derivatives (**7a–c**) with solubilizing alkyl groups as an n-type organic semiconductor. Despite the possible isomers depending on the connectivity between the thiophene and DBP moieties, ¹H NMR spectra and single crystal X-ray analysis clearly showed that only the *EE*-isomer, the least steric congested isomer, was formed. Electrochemical evaluation revealed that their electronic structures are similar to those of terthienoquinoidal derivatives having a similar π -conjugation length, indicating that they have fairly low-lying LUMO energy levels enabling to afford air-stable n-channel OFETs. In fact, their solution-deposited thin films can act as the active semiconducting layer under the ambient conditions with field-effect electron mobility of up to $4.5 \times 10^{-2} \text{cm}^2 \text{V}^{-1} \text{s}^{-1}$, which is almost comparable with or slightly lower than those of related thienoquinoidal derivatives. It is interesting to note that, although the electron mobilities were not significantly affected by the position of the alkyl groups, the mode of intermolecular interaction is affected by the alkylation positions, testified by the thin film absorption spectra, where distinct blue shift was

observed for **7b**, whereas red shift for **7c**. This can be understood by dominant effect of intermolecular van der Waals interaction caused by the long and linear alkyl groups in determining mutual position of the molecules in the thin film state. In fact, such structural change could also bring an emergence of hole transport only in the former thin films, implying enhanced intermolecular orbital overlap of HOMOs, to which the DBP part contributes significantly. A similar topological separation of HOMO and LUMO in the orthogonal manner was already pointed out in aromatic-fused naphthalene diimide system, with which superior ambipolar organic semiconductors have been developed.²⁰ With the present results on the DBP-embedded thienoquinoidal structures, new molecular design and synthesis of efficient ambipolar materials are now underway in our group.

Experimental

Synthesis

General: All chemicals and solvents are of reagent grade unless otherwise indicated. Tetrahydrofuran (THF) was purified with a standard procedure prior to use. 5,10-Bis(5-bromo-4-eicosylthiophen-2-yl)dibenzo[*a,e*]pentalene (**8b**) was synthesized as reported.¹³ Preparation of 5,10-bis(5-bromo-4-hexylthiophen-2-yl)dibenzo[*a,e*]pentalene (**8a**) and 5,10-bis(5-bromothiophen-2-yl)-2,7-di(tetradecyl)dibenzo[*a,e*]pentalene (**8c**) were described in Electronic Supplementary Information (ESI). Melting points were uncorrected. All reactions were carried out under nitrogen atmosphere. Nuclear magnetic resonance spectra were obtained in deuterated chloroform (CDCl₃) with TMS as internal reference unless otherwise stated; chemical shifts (δ) are reported in parts per million. IR spectra were recorded using a KBr pellet. EI-MS spectra were obtained using an electron impact ionization procedure (70 eV). The molecular ion peaks of the bromine or sulphur containing compounds showed a typical isotopic pattern, and all the mass peaks are reported based on ⁷⁷Br and ³²S, respectively. HRMS measurements were carried out at the Natural Science Centre for Basic Research and Development (N-BARD), Hiroshima University.

5,10-Bis(5-iodo-4-hexylthiophen-2-yl)-dibenzo[*a,e*]pentalene (**9a**)

5,10-Bis(5-bromo-4-hexylthiophen-2-yl)dibenzo[*a,e*]pentalene (**8a**, 0.346 g, 0.50 mmol), sodium iodide (0.357 g, 1.0 mmol), copper iodide (10 mg), and *N,N*-dimethyl-cyclohexane-1,2-diamine (0.2 mL) were added to dry 1,4-dioxane (100 mL).¹⁵ The mixture was stirred for 3 h at 110 °C. After evaporation of the solvent, the residue was purified by column chromatography on silica gel eluted dichloromethane/hexane (1:1, v/v) to give **9a** (0.283 g, 72%) as a brown solid: Mp 131–132 °C; ¹H NMR (400 MHz) δ 80.91 (d, $J = 7.6 \text{ Hz}$, 6H), 1.35–1.40 (m, 12H), 1.63 (quin, $J = 7.6 \text{ Hz}$, 4H), 2.62 (t, $J = 7.6 \text{ Hz}$, 4H), 6.93 (d, $J = 7.9 \text{ Hz}$, 2H), 6.96 (s, 2H), 7.24 (d, $J = 6.6 \text{ Hz}$, 2H), 7.25 (d, $J = 6.6 \text{ Hz}$, 2H), 7.56 (d, $J = 6.6 \text{ Hz}$, 2H); ¹³C NMR (100 MHz) δ 14.3, 22.8, 29.1, 30.2, 31.8, 32.5, 122.4,

122.8, 128.0, 128.1, 129.5, 132.6, 134.6, 140.1, 142.9, 148.1, 148.6; EI-MS (70 eV) = 787 (M^+); HRMS (APCI): Calcd for $C_{36}H_{37}I_2S_2$: 787.04206 [MH^+]. Found: 787.04315.

5,10-Bis(5-iodo-4-eicosylthiophen-2-yl)dibenzo[*a,e*]pentalene (9b)

A similar procedure to **9a** using 5,10-bis(5-bromo-4-eicosylthiophen-2-yl)dibenzo[*a,e*]pentalene¹³ gave the title compound in 69% isolated yield: Mp 107–108 °C; ¹H NMR (400 MHz) δ 0.90 (d, J = 7.6 Hz, 6H), 1.25–1.40 (m, 68H), 1.68 (quin, J = 7.6 Hz, 4H), 2.64 (t, J = 7.6 Hz, 4H), 6.93 (t, J = 6.6 Hz, 2H), 6.96 (t, J = 6.6 Hz, 2H), 7.13 (s, 2H), 7.25 (d, J = 6.6 Hz, 2H), 7.56 (d, J = 6.6 Hz, 2H); ¹³C NMR (100 MHz) δ 14.15, 14.17, 22.8, 29.49, 29.51, 29.6, 29.66, 29.70, 29.8, 29.88, 30.3, 32.1, 32.58, 32.61, 122.6, 122.9, 128.1, 128.3, 129.6, 132.8, 134.8, 140.4, 143.3, 148.3, 148.9; HRMS (APCI): Calcd for $C_{64}H_{93}I_2S_2$: 1179.48026, [MH^+]. Found: 1179.48230.

5,10-Bis(5-iodothiophen-2-yl)-2,7-di(tetradecyl)dibenzo[*a,e*]pentalene (9c)

With **8c** a similar procedure from **8a** to **9a** afford 5,10-bis(5-iodothiophen-2-yl)-2,7-di(tetradecyl)dibenzo[*a,e*]pentalene (**9c**) (1.14 g, 1.13 mmol) as a brown solid (90% yield): Mp 122–123 °C; ¹H NMR (400 MHz) δ 0.88 (d, J = 7.4 Hz, 6H), 1.26–1.31 (m, 44H), 1.57 (quin, J = 7.4 Hz, 4H), 2.47 (t, J = 7.4 Hz, 4H), 6.70 (d, J = 7.9 Hz, 2H), 6.99 (s, 2H), 7.11 (d, J = 3.7 Hz, 2H), 7.33 (d, J = 3.7 Hz, 2H), 7.38 (d, J = 7.9 Hz, 2H); ¹³C NMR (100 MHz) δ 14.2, 22.8, 29.5, 29.7, 29.8, 29.89, 29.92, 31.4, 32.1, 36.3, 43.1, 75.3, 117.2, 122.4, 123.2, 127.6, 127.7, 131.5, 132.0, 132.0, 143.8, 143.8; HRMS (APCI): Calcd for $C_{52}H_{69}I_2S_2$: 1011.29246, [MH^+]. Found: 1011.29468.

5,10-Bis[5-(dicyanomethylene)-4-hexyl-2(5*H*)-thienylidene]-5,10-dihydrodibenzo[*a,e*]pentalene (7a)

Under argon atmosphere, sodium hydride (60% in oil, 34 mg, 0.85 mmol) was added into a solution of malononitrile (27 mg, 0.42 mmol) in THF (10 mL), and the mixture was stirred at rt for 30 min. Then, tetrakis(triphenylphosphine)palladium(0) (11 mg, 10 mol%) and 1,1'-bis(diphenylphosphino)ferrocene (dppf, 10 mg) were added to the mixture followed by slow addition of a solution of **9a** (71 mg, 0.09 mmol) in THF (10 mL) was over a period of 30 min. The mixture was refluxed for 15 h, and then hydrochloric acid (2M, 1 mL) was added under ice-cooling. After stirred for 30 min in air, the mixture was extracted with chloroform (30 mL \times 2) to give a dark red solid after concentration. To the crude product was added a solution of 2,3-dichloro-5,6-dicyano-*p*-benzoquinone (98 mg, 0.432 mmol) in acetonitrile (15 mL). After refluxed for 1 h, resulting precipitate was collected by filtration and washed with acetonitrile, water, acetone, and hexane to give **7a** (56 mg, 94% yield): Mp 249–250 °C; ¹H NMR (400 MHz) δ 0.92 (t, J = 7.3 Hz, 6H), 1.34–1.54 (m, 12H), 2.98 (t, J = 7.3 Hz, 2H), 7.29 (t, J = 7.6 Hz, 2H), 7.34 (t, J = 7.6 Hz, 2H), 7.48 (d, J = 7.6 Hz, 2H), 7.83 (d, J = 7.6 Hz, 2H), 7.97 (s, 2H); ¹³C NMR (100 MHz) δ 13.9, 22.5, 28.8, 29.4, 29.5, 31.6, 71.47, 112.8, 114.2, 122.1, 126.3, 127.2, 129.8, 134.8, 136.4, 139.8, 141.3, 148.3, 170.7; IR (KBr) ν = 2210 cm^{-1} (CN) HRMS (APCI): Calcd for $C_{42}H_{37}N_4S_2$: 661.24542 [MH^+]. Found: 661.24561.

5,10-Bis[5-(dicyanomethylene)-4-eicocyl-2(5*H*)-thienylidene]-5,10-dihydrodibenzo[*a,e*]pentalene (7b)

A similar procedure gave the title compound from **9b** in 90% isolated yield: ¹H NMR (400 MHz) δ 0.88 (t, J = 7.3 Hz, 6H), 1.26–1.48 (m, 68H), 1.76 (quin, J = 7.3 Hz, 2H), 2.95 (t, J = 7.3 Hz, 2H), 7.31 (t, J = 7.6 Hz, 2H), 7.35 (t, J = 7.6 Hz, 2H), 7.46 (d, J = 7.6 Hz, 2H), 7.80 (d, J = 7.6 Hz, 2H), 7.94 (s, 2H); ¹³C NMR (100 MHz) δ 14.2, 22.8, 29.3, 29.5, 29.6, 29.7, 29.8, 29.9, 32.1, 72.2, 112.9, 114.3, 122.2, 127.4, 130.0, 134.9, 136.6, 140.1, 141.5, 142.8, 148.5, 166.2; Mp 239–240 °C; IR (KBr) ν = 2211 cm^{-1} (CN); HRMS (APCI): Calcd for $C_{70}H_{93}N_4S_2$: 1053.68362, [MH^+]. Found: 1053.68530.

5,10-Bis[5-(dicyanomethylene)-2(5*H*)-thienylidene]-5,10-dihydro-2,7-di(tetradecyl)dibenzo[*a,e*]pentalene (7c)

With **9c** (76 mg, 0.09 mmol) a similar procedure from **9a** to **7a** afford **7c** (97 mg, 89%): Mp 170–171 °C; ¹H NMR (400 MHz) δ 0.87 (t, J = 7.0 Hz, 6H), 1.24–1.35 (m, 44H), 1.66 (quin, J = 7.0 Hz, 4H), 2.17 (t, J = 7.0 Hz, 2H), 7.15 (d, J = 7.2 Hz, 2H), 7.32 (d, J = 7.2 Hz, 2H), 7.47 (d, J = 5.3 Hz, 2H), 7.57 (s, 2H), 8.24 (d, J = 5.3 Hz, 2H); ¹³C NMR (100 MHz) δ 4.9, 13.6, 20.2, 20.3, 20.32, 20.4, 20.42, 20.6, 22.3, 22.8, 27.0, 63.3, 103.3, 104.2, 113.3, 117.9, 121.1, 122.9, 125.0, 128.2, 132.1, 134.0, 135.0, 163.1; IR (KBr) ν = 2215 cm^{-1} (CN); HRMS (APCI): Calcd for $C_{58}H_{69}N_4S_2$: 885.49582, [MH^+]. Found: 885.49719.

Instrumentation

UV-Vis absorption spectra were measured using a Shimadzu UV-3600 spectrometer. Cyclic voltammograms (CVs) were recorded on an ALS Electrochemical Analyzer Model 612D in dichloromethane containing tetrabutylammonium hexafluorophosphate (Bu_4NPF_6 , 0.1 M) as supporting electrolyte at a scan rate of 100 mV/s. Counter and working electrodes were made of Pt, and the reference electrode was Ag/AgCl. All the potentials were calibrated with the standard ferrocene/ferrocenium redox couple (Fc/Fc^+ : $E_{1/2}$ = +0.44 V measured under identical conditions). X-ray diffractions of thin films deposited on the Si/SiO₂ substrate were obtained with a Rigaku Ultima IV diffractometer with a Cu K α source (λ = 1.541 Å) in the air. Samples for the XRD measurements were prepared by drop-casting the polymer on the OTS-modified Si/SiO₂ substrate. X-ray crystal structure analysis of **7a** was made on a Rigaku R-Axis RAPID (Cu K α radiation, λ = 1.54187 Å, graphite monochromator, T = 93 K). The structure was solved by the direct methods.²¹ Non-hydrogen atoms were refined anisotropically, and hydrogen atoms were included in the calculations but not refined. All calculations were performed using the crystallographic software package CrystalStructures 4.0.²²

Device fabrication and evaluation

OFETs were fabricated in a “top-contact” configuration on a heavily doped n⁺-Si (100) wafer with a 200 nm thermally grown SiO₂ (C_i = 17.3 nF cm^{-2}). The substrate surfaces were treated with octyltrichlorosilane (OTS) as reported previously.²³ Thin-films of the organic semiconductors as the active layer were deposited on the Si/SiO₂ substrates by the spin-coating method. On top of the organic thin film, gold films (80 nm) as

drain and source electrodes were deposited through a shadow mask. For a typical device, the drain-source channel length (L) and width (W) are 50 μm and 1.5 mm, respectively. Characteristics of the OFET devices were measured at room temperature under ambient conditions with a Keithley 4200 semiconducting parameter analyser. Field-effect mobility (μ_{FET}) was calculated in the saturation ($V_{\text{d}} = 60$ V) of the I_{d} using the following equation,

$$I_{\text{d}} = C_i \mu_{\text{FET}} (W/2L) (V_{\text{g}} - V_{\text{th}})^2$$

where C_i is the capacitance of the SiO_2 insulator, and V_{g} and V_{th} are the gate and threshold voltages, respectively. Current on/off ratio ($I_{\text{on}}/I_{\text{off}}$) was determined from the I_{d} at $V_{\text{g}} = 0$ V (I_{off}) and $V_{\text{g}} = 60$ V (I_{on}). The μ_{FET} data reported are typical values from more than ten different devices.

Acknowledgements

This work was financially supported by Grants-in-Aid for Scientific Research (Nos. 23245041 and 25-1759) from MEXT, Japan. HRMSs were carried out at the Natural Science Centre for Basic Research and Development (N-BARD), Hiroshima University. We also thank Rigaku Corp. for the single crystal X-ray analysis. One of the authors (M.N.) is grateful for the Postdoctoral Fellowship of Japan Society for the Promotion of Science (JSPS).

Notes and references

^aEmergent Molecular Function Research Group, RIKEN Center for Emergent Matter Science (CEMS), Wako, Saitama 351-0198, Japan.

^bDepartment of Applied Chemistry, Graduate School of Engineering, Hiroshima University, Higashi-Hiroshima 739-8527, Japan.

† Electronic Supplementary Information (ESI) and crystallographic data available. See DOI: 10.1039/b000000x/

- Organic electronics in general: (a) *Organic Electronics, Manufacturing and Applications*; H. Klauk, Ed.; Wiley-VCH: Weinheim, 2006. (b) *Organic Electronics II, More Materials and Applications*; H. Klauk, Ed.; Wiley-VCH: Weinheim, 2012. (c) A. Facchetti, *Mater. Today*, 2007, **10**, 28–37.
- Z. Bao, J. Locklin., Eds. *Organic Field-Effect Transistors*; CRC Press: Boca Raton, FL, 2007.
- (a) X. Gao, Y. Hu, *J. Mater. Chem. C*, 2014, **2**, 3099–3117. (b) J. E. Anthony, A. Facchetti, M. Heeney, S. R. Marder, X. Zhan, *Adv. Mater.*, 2010, **22**, 3876–3892 (c) H. Usta, A. Facchetti, T. J. Marks, *Acc. Chem. Res.*, 2011, 501–510.
- (a) F. Würthner, M. Stolte, *Chem. Commun.*, 2011, **47**, 5109–5115. (b) S.-L. Suraru, F. Würthner, *Angew. Chem. Int. Ed.*, 2014, **53**, 7428–7448. (c) X. Zhan, A. Facchetti, S. Barlow, T. J. Marks, M. A. Ratner, M. R. Wasielewski, S. R. Marder, *Adv. Mater.*, 2011, **23**, 268–284. (d) M. Sommer, *J. Mater. Chem. C*, 2014, **2**, 3088–3098 (e) Z. Liu, G. Zhang, Z. Cai, X. Chen, H. Luo, Y. Li, J. Wang, D. Zhang, *Adv. Mater.*, in press (f) X. Guo, A. Facchetti, T. J. Marks, *Chem. Rev.*, in press.
- (a) R. C. Haddon, A. S. Perel, R. C. Morris, T. T. M. Palstra, A. F. Hebard, R. M. Fleming, *Appl. Phys. Lett.*, 1995, **67**, 121–123. (b) C. Waldauf, P. Schilinsky, M. Perisutti, J. Hauch, C. J. Brabec, *Adv. Mater.*, 2003, **15**, 2084–2088. (c) Th. B. Singh, N. Marjanovič, P. Stadler, M. Auinger, G. J. Matt, S. Günes, and N. S. Sariciftci, *J. Appl. Phys.*, 2005, **97**, 083714.
- (a) Z. Bao, A. J. Lovinger, J. Brown, *J. Am. Chem. Soc.*, 1998, **120**, 207–208. (b) Y. Sakamoto, T. Suzuki, M. Kobayashi, Y. Gao, Y. Fukai, Y. Inoue, F. Sato, S. Tokito, *J. Am. Chem. Soc.*, 2004, **126**, 8138–8140.
- (a) J. Ferraris, D. O. Cowan, V. Walatka, J. H. Perlstein, *J. Am. Chem. Soc.*, 1973, **95**, 948–949. (b) N. Martin, J. L. Segura, C. Seoane, *J. Mater. Chem.*, 1997, **7**, 1661–1676.
- (a) J. Casado, R. Ponce Ortiz, J. T. Lopez Navarrete, *Chem. Soc. Rev.*, 2012, **41**, 5672–5686. (b) S. Gronowitz, B. Uppström, *Acta Chem. Scand.*, B, 1974, **28**, 981–985. (c) K. Yui, Y. Aso, T. Otsubo, F. Ogura, *J. Chem. Soc., Chem. Commun.*, 1987, 1816–1817. (d) K. Yui, H. Ishida, Y. Aso, T. Otsubo, F. Ogura, *Chem. Lett.* 1987, 2339–2342. (e) K. Yui, Y. Aso, T. Otsubo, F. Ogura, *Bull. Chem. Soc. Jpn.*, 1989, **62**, 1539–1546. (f) K. Yui, H. Ishida, Y. Aso, T. Otsubo, F. Ogura, A. Kawamoto, J. Tanaka, *Bull. Chem. Soc. Jpn.*, 1989, **62**, 1547–1555.
- (a) A. R. Brown, D. M. de Leeuw, E. J. Lous, E. E. Havinga, *Synth. Met.*, 1994, **66**, 257–261. (b) J. G. Laquindanum, H. E. Katz, A. Dodabalapur, A. J. Lovinger, *J. Am. Chem. Soc.*, 1996, **118**, 11331–11332. (c) D. M. de Leeuw, M. M. J. Simenon, A. R. Brown, R. E. F. Einerhand, *Synth. Met.*, 1997, **87**, 53–59. (d) E. Menard, V. Podzorov, S. -H. Hur, A. Gaur, M. E. Gershenson, J. A. Rogers, *Adv. Mater.*, 2004, **16**, 2097–2101. (e) N. Yanai, T. Mori, S. Shinamura, I. Osaka, K. Takimiya, *Org. Lett.*, 2014, **16**, 240–243.
- (a) T. M. Pappenfus, R. J. Chesterfield, C. D. Frisbie, K. R. Mann, J. Casado, J. D. Raff, L. L. Miller, *J. Am. Chem. Soc.*, 2002, **124**, 4184–4185. (b) J. Casado, L. L. Miller, K. R. Mann, T. M. Pappenfus, H. Higuchi, E. Orti, B. Milian, R. Pou-Amerigo, V. Hernandez, J. T. Lopez Navarrete, *J. Am. Chem. Soc.*, 2002, **124**, 12380–12388. (c) R. J. Chesterfield, C. R. Newman, T. M. Pappenfus, P. C. Ewbank, M. H. Haukaas, K. R. Mann, L. L. Miller, C. D. Frisbie, *Adv. Mater.*, 2003, **15**, 1278–1282. (d) A. Berlin, S. Grimoldi, G. Zotti, R. M. Osuna, M. C. Ruiz Delgado, R. P. Ortiz, J. Casado, V. Hernandez, J. T. Lopez Navarrete, *J. Phys. Chem. B*, 2005, **109**, 22308–22318. (e) Y. Kunugi, K. Takimiya, Y. Toyoshima, K. Yamashita, Y. Aso, T. Otsubo, *J. Mater. Chem.*, 2004, **14**, 1367–1369. (f) S. Handa, E. Miyazaki, K. Takimiya, Y. Kunugi, *J. Am. Chem. Soc.*, 2007, **129**, 11684–11685. (g) S. Handa, E. Miyazaki, K. Takimiya, *Chem. Commun.*, 2009, 3919–3921. (h) J. C. Ribierre, T. Fujihara, S. Watanabe, M. Matsumoto, T. Muto, A. Nakao, T. Aoyama, *Adv. Mater.*, 2010, **22**, 1722–1726. (i) Y. Suzuki, E. Miyazaki, K. Takimiya, *J. Am. Chem. Soc.*, 2010, **132**, 10453–10466. (j) Y. Suzuki, M. Shimawaki, E. Miyazaki, I. Osaka, K. Takimiya, *Chem. Mater.*, 2011, **23**, 795–804. (k) J. C. Ribierre, S. Watanabe, M. Matsumoto, T. Muto, D. Hashizume, T. Aoyama, *J. Phys. Chem. C*, 2011, **115**, 20703–20709.
- (a) T. Kashiki, E. Miyazaki, K. Takimiya, *Chem. Lett.*, 2009, **38**, 568–569. (b) Q. Wu, R. Li, W. Hong, H. Li, X. Gao, D. Zhu, *Chem. Mater.*, 2011, **23**, 3138–3140. (c) N. Yanai, T. Mori, S. Shinamura, I. Osaka, K. Takimiya, *Org. Lett.*, 2014, **16**, 240–243. (d) T. Mori, N. Yanai, I. Osaka, K. Takimiya, *Org. Lett.*, 2014, **16**, 1334–1337. (f) G. E. Rudebusch, A. G. Fix, H. A. Henthorn, C. L. Vonnegut, L. N. Zakharov and M. M. Haley, *Chem. Sci.* 2014, **5**, 3627–3633.
- (a) H. Zhong, J. Smith, S. Rossbauer, A. J. P. White, T. D. Anthopoulos, M. Heeney, *Adv. Mater.*, 2012, **24**, 3205–3211. (b) Y.

- Qiao, Y. Guo, C. Yu, F. Zhang, W. Xu, Y. Liu, D. Zhu, *J. Am. Chem. Soc.*, 2012, **134**, 4084–4087. (c) Q. Wu, S. Ren, M. Wang, X. Qiao, H. Li, X. Gao, X. Yang, D. Zhu, *Adv. Funct. Mater.*, 2013, **23**, 2277–2284.
- 13 (a) J. Yang, M. V. Lakshmikantham, M. P. Cava, D. Lorey, J. R. Bethelot, *J. Org. Chem.*, 2000, **65**, 6739–6742. (b) M. Nakano, I. Osaka, K. Takimiya, T. Koganezawa, *J. Mater. Chem. C*, 2014, **2**, 64–70.
- 14 M. Uno, K. Seto, S. Takahashi, *J. Chem. Soc., Chem. Commun.*, 1984, 932–933.
- 15 A. Klapars, S. L. Buchwald, *J. Am. Chem. Soc.*, 2002, **124**, 14844–14845.
- 16 MO calculations were carried out with the DFT/TD-DFT method at the B3LYP/6-31G(d) level using Gaussian 03 program package. Frisch, M. J. *et al.* Gaussian 03, revision C.02; Gaussian, Inc., Wallingford, CT, 2004.
- 17 **7a**-film can be deposited on the Si/SiO₂ substrate by drop-casting from hot *o*-dichlorobenzene solution. Comparison of the out-of-plane and in-plane XRD patterns of the film with the simulated powder pattern from the bulk **7a**-crystal structure suggested that the packing structure and molecular orientation of **7a** in the thin-film should be different from those in the bulk single crystal (Figure S5).
- 18 (a) H. Inokuchi, G. Saito, P. Wu, K. Seki, T. B. Tang, T. Mori, K. Imaeda, T. Enoki, Y. Higuchi, K. Inaka, N. Yasuoka, *Chem. Lett.*, 1986, **15**, 1263–1266. (b) H. Ebata, T. Izawa, E. Miyazaki, K. Takimiya, M. Ikeda, H. Kuwabara, T. Yui, *J. Am. Chem. Soc.*, 2007, **129**, 15732–15733.
- 19 A. Mishra, R. K. Behera, P. K. Behera, B. K. Mishra, G. B. Behera, *Chem. Rev.*, 2000, **100**, 1973–2012.
- 20 (a) S.-L. Suraru, U. Zschieschang, H. Klauk, F. Würthner, *Chem. Commun.*, 2011, **47**, 11504–11506. (b) Y. Fukutomi, M. Nakano, J.-Y. Hu, I. Osaka, K. Takimiya, *J. Am. Chem. Soc.*, 2014, **135**, 11445–11448.
- 21 M. C. Burla, R. Caliendo, M. Camalli, B. Carrozzini, G. L. Cascarano, L. De Caro, C. Giacovazzo, G. Polidori, D. Siliqi, R. Spagna, *J. Appl. Cryst.*, 2007, **40**, 609–613.
- 22 Rigaku (2011). CrystalStructure. Version 4.0. Rigaku Corporation, Tokyo, Japan.
- 23 B. S. Ong, Y. Wu, P. Liu, S. Gardner, *J. Am. Chem. Soc.*, 2004, **126**, 3378–3379.

